Graphene p–n Vertical Tunneling Diodes

Sung Kim,[†,§] Dong Hee Shin,[†,§] Chang Oh Kim,[†] Soo Seok Kang,[†] Jong Min Kim,[†] Chan Wook Jang,[†] Soong Sin Joo,[†] Jae Sung Lee,[†] Ju Hwan Kim,[†] Suk-Ho Choi,[†,*] and Euyheon Hwang[‡]

[†]Department of Applied Physics, College of Applied Science, Kyung Hee University, Yongin 446-701, Korea, and [‡]SKKU Advanced Institute of Nanotechnology, Sungkyunkwan University, Suwon 440-746, Korea. [§]S. Kim and D. H. Shin contributed equally to this work.

ABSTRACT Formation and characterization of graphene p–n junctions are of particular interest because the p–n junctions are used in a wide variety of electronic/photonic systems as building blocks. Graphene p–n junctions have been previously formed by using several techniques, but most of the studies are based on lateral-type p–n junctions, showing no rectification behaviors. Here, we report a new type of graphene p–n junction. We first fabricate and characterize vertical-type graphene p–n junctions with two terminals. One of the most important characteristics of the vertical junctions is the asymmetric rectifying behavior showing an on/off ratio of $\sim 10^3$ under bias voltages below ± 10 V without gating at higher n doping concentrations, which may be useful for practical device applications. In contrast, at lower n doping concentrations, the p–n junctions are ohmic, consistent with the Klein-tunneling effect. The observed rectification results possibly from the formation of strongly corrugated insulating or semiconducting interlayers between the metallic p- and n-graphene sheets at higher n doping concentrations, which is actually a structure like a metal–insulator–metal or metal–semiconductor–metal tunneling diode. The properties of the diodes are almost invariant even 6 months after fabrication.

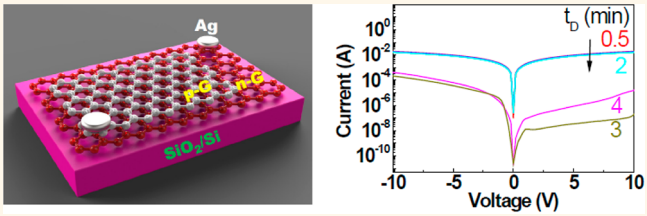

KEYWORDS: graphene · p–n diode · vertical junction · tunneling · asymmetric · rectification · interlayer

Recently, graphene has been considered as one of the most promising materials candidates for post-silicon electronics.[1,2] Modulation of electrical and optical properties in graphene is of great importance to realize graphene-based electronics/photonics. Doping of graphene provides a simple way to control its characteristics because the doping leads to a shift of the Fermi level. There have been considerable studies on the doping of graphene by using electrochemical,[3,4] electrostatic,[5,6] or chemical techniques,[7–9] but the former two methods have drawbacks of having an influence of high voltage on the properties of the substrate or requiring a specific electrochemical setup, respectively. Surface transfer or substitutional doping of graphene with foreign atoms (*i.e.*, impurities), which is of critical importance for its applications to practical devices, has been studied by chemical doping.[7–9]

Various methods, such as multiple electrostatic gating,[5,10] local chemical treatment,[11,12] and electrostatic substrate engineering,[13] have been employed to form graphene p–n junctions, most of which are lateral type. It is fundamentally known that lateral graphene p–n junctions cannot show rectifying behaviors due to the Klein-tunneling effect,[14] thereby limiting their applications. The air stability of n-type graphene, one of the biggest issues in current graphene studies,[15] should be also overcome to achieve long-term-stable p–n junctions. On the other hand, electrical transport through vertical graphene heterostructures with BN or Al_2O_3 barriers without real doping of graphene has been recently realized for field-effect[16] and hot-electron[17] tunneling transistors with three terminals.

It has been reported that the sheet resistance increases by doping of benzyl viologen (BV) for n-type graphene,[9] contrary to common sense. Thus, the mobility of BV-doped n-type graphene will decrease for higher doping because the electron density increases by doping. If this doping method is available for enhancing the resistance of the interface between p- and n-type graphene sheets, it could be possible to fabricate graphene-based metal–insulator–metal

* Address correspondence to sukho@khu.ac.kr.

Received for review February 22, 2013 and accepted May 21, 2013.

Published online May 21, 2013
10.1021/nn400899v

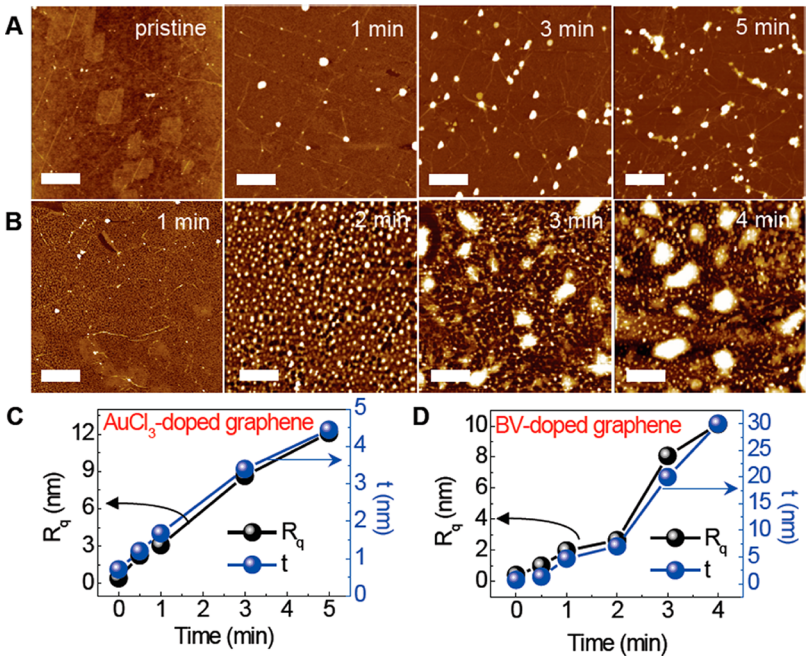

Figure 1. AFM topographic images of (A) $AuCl_3$- and (B) BV-doped graphene sheets for various doping times. Here, the scale bars indicate 2 μm. Roughness (R_q) and thickness (t) of (C) $AuCl_3$- and (D) BV-doped graphene sheets as functions of doping time.

(MIM) or metal−semiconductor−metal (MSM) tunneling diodes. In this work, we propose a vertical graphene p−n junction, which has not been studied yet in the literature to our knowledge. We prepare n-and p-type graphene sheets by chemical doping of $AuCl_3$ and BV, respectively, optimize their characteristics, and realize graphene p−n vertical tunneling diodes with two terminals, showing rectifying behaviors stable in air for more than 6 months, much more simple in operation as well as in structure for practical device applications than the previous graphene vertical structures with three terminals including a gate.[16,17]

RESULTS AND DISCUSSION

For doping of graphene, the dopant solution was dropped on the graphene sheet, and after some time (this time is defined as doping time, t_D) elapsed, it was spin-coated. The t_D was varied to change the doping concentration (see the Experimental Section). The atomic force microscopy (AFM) images in Figure 1A and B show the effects of t_D on the surface morphologies of $AuCl_3$- and BV-doped graphene sheets, respectively. The pristine graphene used for the doping was demonstrated to be single layer by the AFM height profile of the step at the graphene/bare SiO_2, and the roughness (R_q) and thickness (t) of the doped graphene sheets were similarly measured (see Supporting Information Figures S1 and S2). The AFM images of the $AuCl_3$-doped graphene sheets show that the graphene surfaces become gradually roughened as t_D increases, and correspondingly, the R_q and t estimated by AFM height profiles are proportional to t_D, as shown in Figure 1C. The surface roughness can be attributed to the formation of Au particles due to the higher reduction potential of the $AuCl_4^-$ ion (1.0 V) compared to that of graphene (0.22 V).[18] Figure 1B shows that the surface corrugation was greatly enhanced by long-time BV doping (t_D > 2 min). For $t_D \leq 2$ min, the R_q and t of BV-doped graphene gradually increase with increasing t_D, but above t_D = 2 min, they sharply increase to ~10 and ~30 nm, respectively, with increasing t_D up to 4 min, as shown in Figure 1D.

Figure 2A shows the effect of doping time on Raman spectra of n- and p-type graphene sheets. Two distinctive features in the Raman spectra are G and 2D peaks at ~1580 and ~2700 cm^{-1}, involving phonons at the Γ and K points, respectively.[19] A relatively small Raman feature at ~1350 cm^{-1} is identified with a disorder-induced band or D band. Evidence of the charge transfer has been detected from the G- and 2D-band shifts due to the phonon stiffening.[3] Figure 2B summarizes the shifts of the G and 2D bands. The data measured from 20 different spots with a laser excitation energy of 532 nm (2.33 eV) were averaged to obtain the Raman-peak wavenumbers. With increasing doping time, both G and 2D bands of the n-/p-type graphene sheets shift in the downward/upward directions, respectively, consistent with the previous reports.[20,21]

The average Raman intensity ratios of the G to 2D peaks (determined by the number of stacked graphene layers) and D to G peaks (measure of disorder), defined as ⟨G/2D⟩ and ⟨D/G⟩, respectively, are calculated and plotted as functions of doping time in Figure 2C.

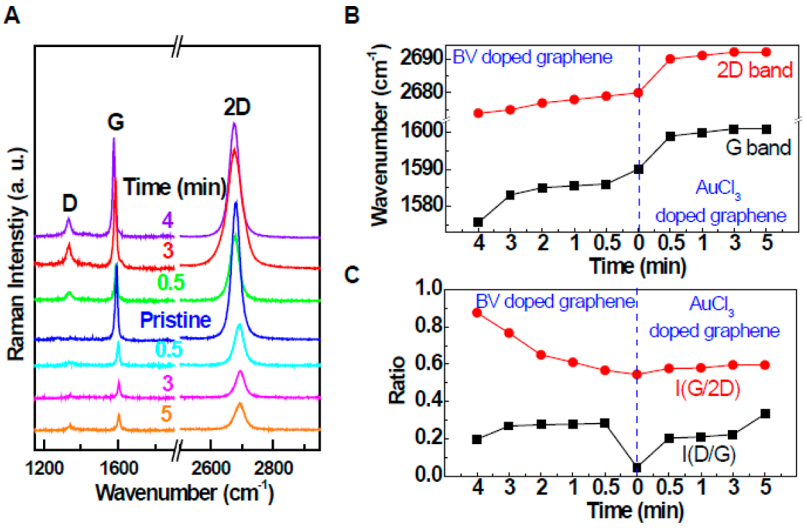

Figure 2. (A) Raman spectra of $AuCl_3$- and BV-doped graphene sheets for various doping times. (B) Peak wavenumbers of 2D and G peaks as functions of doping time for $AuCl_3$- and BV-doped graphene sheets. (C) Average intensity ratios of the G to 2D peaks and D to G peaks as functions of doping time for $AuCl_3$- and BV-doped graphene sheets.

The ⟨G/2D⟩ of p-type graphene shows a slight increase with increasing doping time, indicating a small increase in thickness after p-type doping, but in case of n-type doping, the thickness of graphene shows a great increase with increasing t_D above 2 min, consistent with the variation of the AFM height profiles, as shown in Figure 1D. Figure 2C also shows an increase in the defect density of graphene sheets after doping, irrespective of the doping type, but does not show clear t_D dependence of the defect density.

X-ray photoelectron spectroscopy (XPS) studies also demonstrated successful doping of Au or N into graphene by $AuCl_3$ or BV exposure, respectively (see Supporting Information Figures S3 and S4).

Chemical doping of graphene by $AuCl_3$ or BV exposure shifts the position of the Dirac point in the $I_{ds}-V_g$ (source/drain current−gate voltage) curves of the field-effect transistors (FETs) toward positive or negative gate voltage, respectively, as shown in Figure 3A. These behaviors can be attributed to charge transfer from adsorbed Au or N to graphene, indicating p- or n-type doping, respectively, as similarly discussed for several kinds of doped graphene sheets in the previous reports.[7,22] Figure 3B summarizes shifts of the Dirac point as functions of doping time for the n-and p-type graphene FETs. The doping effect looks stronger in the n-type graphene than in the p-type graphene. The Dirac point of the pristine graphene is shifted to a positive voltage, indicating p-type, possibly resulting from the adsorption of the air molecules.[23,24] This could explain why the doping effect looks stronger in BV-doped graphene. As estimated from the $I_{ds}-V_g$ curves, the electron mobility of graphene is reduced from ~1030 to ~580 $cm^2/(V\ s)$ by BV exposure for 4 min, while almost no variation in the hole mobility is observed by $AuCl_3$ exposure, irrespective of t_D.

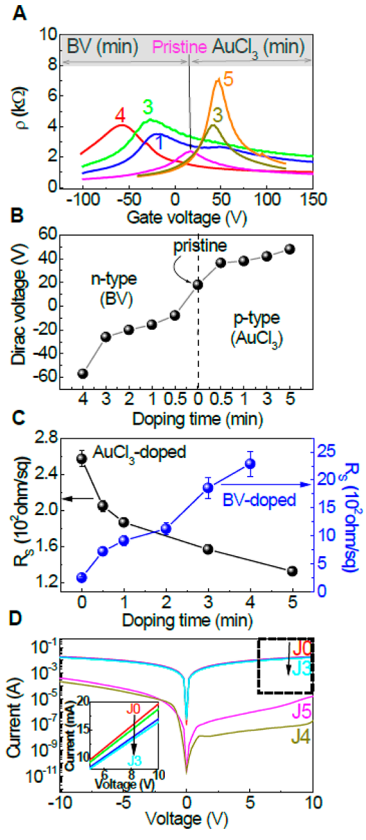

Figure 3. (A) Current−voltage ($I-V$) characteristics of FETs containing $AuCl_3$- or BV-doped graphene for various doping times. (B) Shifts of the Dirac point as a function of doping times for both doping-type graphene FETs. (C) Sheet resistances of $AuCl_3$- and BV-doped graphene sheets as a function of doping time. (D) $I-V$ characteristics of the J0−J5 graphene p−n junction devices. The doping time for the BV exposure was 0.5, 1, 2, 3, and 4 min for J1−J5 devices, respectively, while the doping time for the $AuCl_3$ exposure was fixed at 5 min. The J0 device was formed between pristine graphene sheets for comparison. The inset shows a magnified version of the $I-V$ characteristics under positive bias for J0−J3 devices.

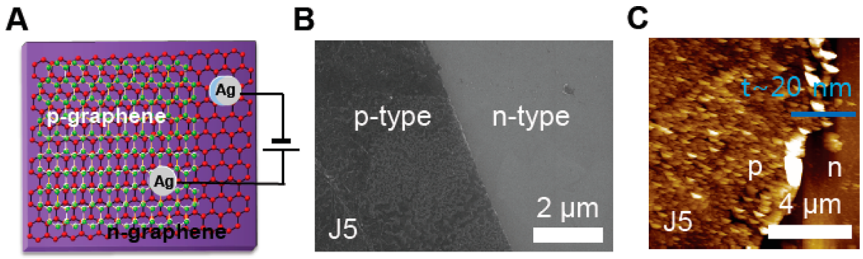

Figure 4. (A) Schematic and (B, C) SEM/AFM images of a typical graphene p−n vertical junction where the doping times of the p and n layers are 5 and 4 min, respectively.

Figure 3C shows sheet resistance of $AuCl_3$- and BV-doped graphene sheets. The sheet resistance of $AuCl_3$-doped graphene monotonically decreases down to ~130 ohm/sq with increasing t_D up to 5 min, consistent with the previous report.[9] The sheet resistance of BV-doped graphene greatly increases up to ~2200 ohm/sq with increasing t_D up to 4 min, in strong contrast with the case of the $AuCl_3$ doping. These results suggest the strongly corrugated structures formed on the surface of the BV-doped graphene at larger t_D, as shown in Figure 1, consist of semiconducting or insulating materials whose major components are C, N, O, and Cl atoms, as detected by XPS (see Supporting Information Figure S4). The transmittance at a wavelength of 550 nm was reduced by only about 5% for the highest n-/p-type doping times (see Supporting Information Figure S5).

We prepared graphene p−n vertical junctions for various doping concentrations of the n-type graphene layer by varying t_D in the BV exposure, while the doping time was fixed at 5 min in the $AuCl_3$ exposure. (For details, see the Experimental Section and Supporting Information Figure S6.) Figure 4A shows a schematic of a typical graphene p−n junction. The devices were named J1−J5 when t_D in the BV exposure was 0.5, 1, 2, 3, and 4 min, respectively. The junction between pristine graphene layers was also formed for comparison and named J0. A scanning electron microscopy (SEM) image demonstrated that the p-type region at the top of the p−n junction was well separated from the bare n-type region at the bottom, as shown in Figure 4B. The AFM image showed there was a ~20 nm step across the p−n junction due to the doping-enhanced roughness (see Figure 4C). The device can be expected to be more sensitive to varying the n-doping time rather than the p-doping time because the n-type graphene is not exposed to air, thereby making it less vulnerable to adsorption effects. This explains why the doping time of n-type graphene was varied at a fixed doping time of p-type graphene in forming the p−n junctions in this work.

Raman spectra were also measured as functions of BV doping time for the top p-type graphene and the bottom n-type graphene after the p−n junction was formed (see Supporting Information Figure S7). Compared to the results in Figure 2B and C, there were little variations in t_D-dependent peak wavenumbers and the intensity ratios on the bare n-type graphene in the devices simply because this was actually not different from the separate n-type graphene sheet. The p-type graphene in the devices showed similar doping concentration dependence of the 2D-peak wavenumber compared to the case without the junction, possibly resulting from the interaction with the n-type graphene in the junction. In contrast, the G-peak wavenumber of the p-type graphene showed little t_D dependence. The ⟨G/2D⟩ ratio of the p-type graphene showed a big increase with increasing t_D, indicating greatly enhanced roughness of the p-type graphene by the interaction with the n-type graphene. However, the defect density of the p-type graphene was almost independent of the junction formation, judging from the small t_D-dependent variation of the ⟨D/G⟩ ratio.

Figure 3D shows current−voltage (I−V) characteristics of the p−n vertical junctions. The I−V curves are symmetric and linear in the forward/reverse directions with respect to zero voltage for J0 to J3 devices, indicating no rectifying behaviors at the p−n junctions, as also confirmed in the their linear plots (see Supporting Information Figure S8). As shown in the inset, only slight variations in the shapes of the I−V curves are observed with increasing t_D up to 2 min (from J1 to J3 devices). However, for a t_D above 2 min (J4 and J5 devices), the current is greatly reduced over the full range of bias voltage, with the current reduction being stronger under forward bias than under reverse bias. The forward- and reverse-biased parts of the I−V curves look inverted in view of conventional diode properties. Moreover, the I−V curves of J4 and J5 devices show nonlinear properties with varying bias voltage, indicating rectifying behaviors (see also Figure S8). Ohmic properties of the metal electrodes were demonstrated for all combinations of graphene junctions used in this work (see Supporting Information Figure S9).

Considering the t_D-dependent thickness variation of the n-graphene, as shown in Figure 1, simple circuitries of the biased p−n junction devices are shown

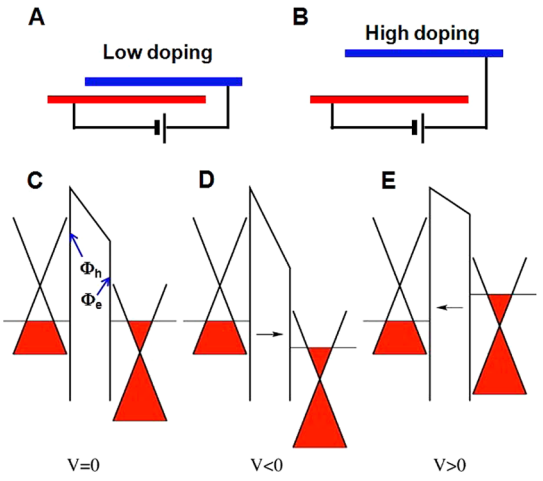

Figure 5. Schematics of the p−n junction devices for (A) low n doping (J1−J3) and (B) high n doping (J4 and J5). Band diagrams of the J4 and J5 p−n junction devices at (C) zero bias, (D) reverse bias, and (E) forward bias. In (C), Φ_h and Φ_e are the work functions of p- and n-type graphene, respectively, and arrows in (D) and (E) indicate the directions of electrons in the presence of reverse and forward biases, respectively.

in Figure 5A and B for low (J1−J3) and high (J4 and J5) n doping, respectively. The symmetric linearity is observed in the *I*−*V* curves of the J1−J3 devices, as shown in Figure 3D. For these junctions two graphene layers are very close and the potential barrier at the boundary of the p−n junction is negligible. As a consequence, the current is governed by Klein tunneling, as shown in the previous reports for the lateral p−n junctions.[25] In contrast, for the J4 and J5 devices the *I*−*V* characteristics are nonlinear and asymmetric, showing anomalous rectifying behaviors with an on/off ratio of $\sim 10^3$ under bias voltages below ±10 V without gating. In the above discussion, strongly corrugated insulating or semiconducting structures were shown to exist on the surface of the n-type graphene layers with t_D = 3 and 4 min, thereby possibly forming insulating or semiconducting interlayers between the metallic p- and n-graphene layers in the J4 and J5 devices, consistent with the film-type deposition of BV, as reported before.[26] This suggests that the J4 and J5 devices actually have a structure similar to an MIM or MSM diode, known to show rectifying *I*−*V* behaviors.[27,28] The p−n vertical tunneling diodes are much more simple in operation as well as in structure than the previous graphene vertical heterostructures[16] because the latter ones have three terminals including a gate and provide gate voltages more than ±50 V for exhibiting *I*−*V* properties with an on/off ratio of $\sim 10^4$. We also studied long-term stabilities of the diode performance by measuring the *I*−*V* curves for 6 months in air, but found no evidence of time-dependent degradation of the diodes (see Supporting Information Figure S10).

Figure 5C−E show possible band diagrams of the J4 and J5 devices depending on the bias. Under zero bias, the p−n junction is at equilibrium, resulting in a negligible current, as shown in Figure 5C. Under reverse bias (negative bias), the Fermi level of the n-graphene goes down and the electrons flow from p-graphene into n-graphene, resulting in a current. Under forward bias (positive bias), the Fermi level of the n-graphene goes up and the electrons flow from the n-graphene into the p-graphene. The transport of electrons at the interlayer region may be induced by the thermionic emission above the barrier and the direct tunneling through the barrier. However, at low temperatures, we expect that the thermionic emission is very small and tunneling processes can dominate the transport. Both J4 and J5 devices exhibit breakdown at ~ -0.2 V without almost no leakage current, as can be seen in the linear plots of the *I*−*V* curves (see Supporting Information Figure S9), consistent with the mechanism of the tunneling diode.[29]

The observed asymmetric current between positive and negative bias can be explained by the linear energy dispersion of graphene (or equivalently linear density of states). In the presence of bias a tunneling current across the potential barrier can be expressed as

$$J(V) \propto \int d\varepsilon D_h(\varepsilon)\, D_e(\varepsilon - eV)\, T(\varepsilon)[f_h(\varepsilon) - f_e(\varepsilon - eV)]$$

where D_h (D_e) and f_h (f_e) are the density of states and the Fermi distribution function of p-type (n-type) graphene, respectively, and T is the tunneling probability. Thus, the tunneling current is mainly determined by the joint density of states, *i.e.*, D_hD_e.

For reverse bias the electrons below the Fermi energy of p-type graphene tunnel to the available states above the Fermi energy of n-type graphene. In this tunneling process the available joint density of states increases. However, for forward bias the electrons below the Fermi energy of n-type graphene tunnel to above the Fermi energy of p-type graphene; that is, electrons tunnel to states close to the Dirac point in p-type graphene, where the available density of states vanishes. Thus the tunneling current for forward bias is much smaller than that for reverse bias, consistent with the asymmetric rectifying *I*−*V* curves of J4 and J5 devices, as shown in Figure 3D. Interestingly the tunneling current may decrease as the forward bias increases when the joint density of states has a minimum, as shown for J4 device in Figure 3D. For a J5 device, a similar current minimum was observed at lower temperature (see Supporting Information Figure S11), possibly resulting from larger thermionic emission in the J5 device due to the lower barrier. However, such a phenomenon does not happen for reverse bias; in this case the joint density of states increases as the bias increases. Another reason for asymmetric current may arise from the change of interfacial potential barrier under different directions of bias. For reverse bias the n-graphene is at a lower

potential and the interfacial insulating barrier width becomes narrower than that of the unbiased case, which gives rise to more current because the electrons go through a lower barrier height or a shorter tunneling distance. In contrast, for forward bias the current would be much smaller due to the increase of the width of the interfacial potential barrier. We calculated the tunneling current as a function of applied bias voltage based on the above equation, incorporating all features we have discussed above. The local minimum of current for positive bias arises at a point minimizing the joint density of states (see Supporting Information Figure S12).

If the n-graphene is doped at a higher concentration, more current is induced under forward bias because the electrons go through a lower barrier height or a shorter tunneling distance due to the higher location of the Fermi level in the n-graphene. In contrast, such current enhancement would be much smaller under reverse bias due to no change of doping concentration in the p-graphene, also consistent with the *I*−*V* curves of J4 and J5 in Figure 3D.

CONCLUSION

We successfully fabricated graphene p−n vertical junctions by varying the n doping concentration, while the p doping concentration was fixed at the highest point. The p−n junction diodes showed asymmetric rectifying behaviors with an on/off ratio of $\sim 10^3$ without gating at higher n doping concentrations, possibly resulting from actual formation of a structure like an MIM or MSM diode. The achievement of the graphene p−n diodes will open exciting opportunities for the creation of all-graphene electrical and optical devices for transparent and flexible electronics and photonics.

EXPERIMENTAL SECTION

The graphene films were prepared by chemical vapor deposition and subsequently transferred to the 300 nm SiO_2/p-type Si wafers. Gold chloride ($AuCl_3$) powder and 1,1′-dibenzyl-4,4′-bipyridinium dichloride (benzyl viologen, BV^{2+}) (Sigma-Aldrich) were used for p- and n-type dopants, respectively. $AuCl_3$ powder was dissolved in nitromethane to yield a 10 mM solution, and BV^{2+} was reduced in a biphasic solution of water/toluene to prepare the 10 mM BV^0 solution.[30] For the doping of graphene, the dopant solution was dropped on the whole surface of the graphene sheet, and after some time (this time is defined as doping time, t_D) elapsed, it was spin-coated at 2000 rpm for 1 min. The t_D was varied to change the doping concentration.

For the formation of the graphene p−n junction, a solution of BV was first dropped and spin-coated on the 10 × 10 mm^2 graphene/SiO_2/p-type Si wafer and then annealed at 100 °C for 10 min to make graphene uniformly n-type. The annealing temperature was optimized through repeated experiments for good-quality doped graphene. Subsequently, a 5 × 5 mm^2 bare graphene was transferred on ∼1/4 area of the n-graphene/SiO_2/p-type Si wafer, and a solution of $AuCl_3$ was dropped and spin-coated on the surface of the graphene and similarly annealed. As a result, a graphene p−n vertical junction was formed on the ∼1/4 area of the SiO_2/p-type Si wafer. Ag electrodes of 1 mm diameter and 1 μm thickness were deposited on the top of both n- and p-graphene layers to complete the graphene p−n device. For the FET structure, Cr/Au source and drain electrodes of 30/10 μm in width/length were fabricated on top of graphene *via* processes including reactive ion etching, metal deposition, and lift-off, similar to those in the previous publications.[3,31]

The topographic image and height profile of graphene were obtained in a noncontact mode of AFM (Park system, model XE-100). Raman spectroscopy with an excitation wavelength of 532 nm was used to characterize the optical properties of graphene films. The atomic bonding states of the doped graphene were characterized by XPS using an Al Kα line of 1486.6 eV. *I*−*V* measurements to characterize the electrical behaviors of graphene p−n junctions and FETs were carried out at room temperature using an Agilent 4156C parameter analyzer. The sheet resistance of the doped graphene sheets was measured at room temperature by the four-probe van der Pauw method.

Conflict of Interest: The authors declare no competing financial interest.

Acknowledgment. We are grateful to Prof. Philip Kim at Columbia University for his helpful discussions. This work was supported by a National Research Foundation of Korea (NRF) grant funded by the Korean government (Ministry of Education, Science and Technology, MEST, No. 2011-0017373).

Supporting Information Available: Additional information for the experimental details on doping of graphene, fabrication of p−n devices, and measurements. This material is available free of charge *via* the Internet at http://pubs.acs.org.

REFERENCES AND NOTES

1. Schwierz, F. Graphene Transistor. *Nat. Nanotechnol.* **2010**, *5*, 487–496.
2. Williams, J. R.; DiCarlo, L.; Marcus, C. M. Quantum Hall Effect in a Gate-Controlled p-n Junction of Graphene. *Science* **2007**, *317*, 638–641.
3. Das, A.; Pisana, S.; Chakraborty, B.; Piscanec, S.; Saha, S. K.; Waghmare, U. V.; Novoselov, K. S.; Krishnamurthy, H. R.; Geim, A. K.; Ferrari, A. C.; *et al.* Monitoring Dopants by Raman Scattering in an Electrochemically Top-Gated Graphene Transistor. *Nat. Nanotechnol.* **2008**, *3*, 210–215.
4. Kalbac, M.; Reina-Cecco, A.; Farhat, H.; Kong, J.; Kavan, L.; Dresselhaus, M. S. The Influence of Strong Electron and Hole Doping on the Raman Intensity of Chemical Vapor-Deposition Graphene. *ACS Nano* **2010**, *4*, 6055–6063.
5. Huard, B.; Sulpizio, J. A.; Stander, N.; Todd, K.; Yang, B.; Goldhaber-Gordon, D. Transport Measurements across a Tunable Potential Barrier in Graphene. *Phys. Rev. Lett.* **2007**, *98*, 236803.
6. Freitag, M.; Steiner, M.; Martin, Y.; Perebeinos, V.; Chen, Z. H.; Tsang, J. C.; Avouris, P. Energy Dissipation in Graphene Field-Effect Transistors. *Nano Lett.* **2009**, *9*, 1883–1888.
7. Liu, H.; Liu, Y.; Zhua, D. Chemical Doping of Graphene. *J. Mater. Chem.* **2011**, *21*, 3335–3345.
8. Ristein, J. Surface Transfer Doping of Semiconductors. *Science* **2006**, *313*, 1057–1058.
9. Shin, H.-J.; Choi, W. M.; Choi, D.; Han, G. H.; Yoon, S.-M.; Park, H.-K.; Kim, S.-W.; Jin, Y. W.; Lee, S. Y.; Kim, J. M.; *et al.* Control of Electronic Structure of Graphene by Various Dopants and Their Effects on a Nanogenerator. *J. Am. Chem. Soc.* **2010**, *132*, 15603–15609.
10. Özyilmaz, B.; Jarillo-Herrero, P.; Efetov, D.; Abanin, D. A.; Levitov, L. S.; Kim, P. Electronic Transport and Quantum Hall Effect in Bipolar Graphene p-n-p Junctions. *Phys. Rev. Lett.* **2007**, *99*, 166804.
11. Peters, E. C.; Lee, E. J.; Burghard, H. M.; Kern, K. Gate Dependent Photocurrents at a Graphene p-n Junction. *Appl. Phys. Lett.* **2010**, *97*, 193102.

12. Farmer, D. B.; Lin, Y.-M.; Afzali-Ardakani, A.; Avouris, P. Behavior of a Chemically Doped Graphene Junction. *Appl. Phys. Lett.* **2009**, *94*, 213106.
13. Chiu, H.-Y.; Perebeinos, V.; Lin, Y.-M.; Avouris, P. Controllable p-n Junction Formation in Monolayer Graphene Using Electrostatic Substrate Engineering. *Nano Lett.* **2010**, *10*, 4634–4639.
14. Young, A. F.; Kim, P. Quantum Interference and Klein Tunnelling in Graphene Heterojunctions. *Nat. Phys.* **2009**, *5*, 222–226.
15. Some, S.; Kim, J.; Lee, K.; Kulkarni, A.; Yoon, Y.; Lee, S.; Kim, T.; Lee, H. Highly Air-Stable Phosphorus-Doped n-Type Graphene Field-Effect Transistors. *Adv. Mater.* **2012**, *24*, 5481–5486.
16. Georgiou, T.; Katsnelson, M. I.; Eaves, L.; Morozov, S. V.; Peres, N. M. R.; Leist, J.; Geim, A. K.; Novoselov, K. S.; Ponomarenko, L. A. Field-Effect Tunneling Transistor Based on Vertical Graphene Heterostructures. *Science* **2012**, *335*, 947–950.
17. Vaziri, S.; Lupina, G.; Henkel, C.; Smith, A. D.; Östling, M.; Dabrowski, J.; Lippert, G.; Mehr, W.; Lemme, M. C. A Graphene-Based Hot Electron Transistor. *Nano Lett.* **2013**, *13*, 1435–1439.
18. Shan, B.; Cho, K. J. First Principles Study of Work Functions of Single Wall Carbon Nanotubes. *Phys. Rev. Lett.* **2005**, *94*, 236602.
19. Ferrari, A. C.; Meyer, J. C.; Scardaci, V.; Casiraghi, C.; Lazzeri, M.; Mauri, F.; Piscanec, S.; Jiang, D.; Novoselov, K. S.; Roth, S.; *et al*. Raman Spectrum of Graphene and Graphene Layers. *Phys. Rev. Lett.* **2006**, *97*, 187401.
20. Kim, K. K.; Bae, J. J.; Kim, S. M.; Park, H. K.; An, K. H.; Lee, Y. H. Control of P-Doping on Single-Walled Carbon Nanotubes with Nitronium Hexafluoroantimonate in Liquid Phase. *Phys. Status Solidi B* **2009**, *246*, 2419–2422.
21. Rao, A. M.; Eklund, P. C.; Bandow, S.; Thess, A.; Smalley, R. E. Evidence for Charge Transfer in Doped Carbon Nanotube Bundles from Raman Scattering. *Nature* **1997**, *388*, 257–259.
22. Farmer, D. B.; Golizadeh-Mojarad, R.; Perebeinos, V.; Lin, Y.-M.; Tulevski, G. S.; Tsang, J. C.; Avouris, P. Evidence for Charge Transfer in Doped Carbon Nanotube Bundles from Raman Scattering. *Nano Lett.* **2009**, *9*, 388–392.
23. Wang, S.; Ang, P. K.; Wang, Z.; Tang, A. L. L.; Thong, J. T. L.; Loh, K. P. High Mobility, Printable, and Solution-Processed Graphene Electronics. *Nano Lett.* **2010**, *10*, 92–98.
24. Kim, B. J.; Jang, H.; Lee, S.-K.; Hong, B. H.; Ahn, J.-H.; Cho, J. H. High-Performance Flexible Graphene Field Effect Transistors with Ion Gel Gate Dielectrics. *Nano Lett.* **2010**, *10*, 3464–3466.
25. Cheng, H.-C.; Shiue, R.-J.; Tsai, C.-C.; Wang, W.-H.; Chen, Y.-T. High-Quality Graphene p-n Junctions *via* Resist-Free Fabrication and Solution-Based Noncovalent Functionalization. *ACS Nano* **2010**, *5*, 2051–2059.
26. Gao, L.-P.; Wei, J.; Wang, Y.-C.; Ding, G.-J.; Yang, Y.-L. A New Repeatable, Optical Writing and Electrical Erasing Device Based on Photochromism and Eelectrochromism of Viologen. *Smart Mater. Struct.* **2012**, *21*, 085006.
27. Grossman, E. N.; Harvey, T. E.; Reintsema, C. D. Controlled Barrier Modification in Nb/NbO_x/Ag Metal Insulator Metal Tunnel Diodes. *J. Appl. Phys.* **2002**, *91*, 10134.
28. Li, D.; Sun, X.; Song, H.; Li, Z.; Jiang, H.; Chen, Y.; Miao, G.; Shen, B. Effect of Asymmetric Schottky Barrier on GaN-Based Metal-Semiconductor-Metal Ultraviolet Detector. *Appl. Phys. Lett.* **2011**, *99*, 261102.
29. Esaki, L. Discovery of the Tunnel Diode. *IEEE Trans. Electron Devices* **1976**, *23*, 644–647.
30. Kim, S. M.; Jang, J. H.; Kim, K. K.; Park, H. K.; Bae, J. J.; Yu, W. J.; Lee, I. H.; Kim, G.; Loc, D. D.; Kim, U. J.; *et al*. Reduction-Controlled Viologen in Bisolvent as an Environmentally Stable n-Type Dopant for Carbon Nanotubes. *J. Am. Chem. Soc.* **2009**, *131*, 327–331.
31. Pisana, S.; Lazzeri, M.; Casiraghi, C.; Novoselov, K. S.; Geim, A. K.; Andrea, C.; Ferrari, A. C.; Mauri, F. Breakdown of the Adiabatic Born-Oppenheimer Approximation in Graphene. *Nat. Mater.* **2007**, *6*, 198–201.